# Novel pMUT-based Acoustic Duplexer for Underwater and Intrabody Communication

Flavius V. Pop*†, Bernard Herrera*, Cristian Cassella*, Guofeng Chen*,
Emrecan Demirors*, Raffaele Guida*, Tommaso Melodia* and Matteo Rinaldi*
*Department of Electrical and Computer Engineering, Northeastern University, Boston USA
†e-mail: flavius.pop@ieee.org

***Abstract*—This work demonstrates for the first time an acoustic duplexer based on Aluminum Nitride pMUTs as radiating elements. The duplexer has the function of efficiently separating independent data-streams coming from the transmit and receive modules while minimizing the noise injected in the channel through the achievement of large out-of-band rejections. As a result, this permits to reach levels of Bit-Error-Rates (BER) that are comparable to those achieved through the use of commercial Lead Zirconate Titanate (PZT) transducers. Furthermore, the simultaneous use of two communication bands allows much higher data-rates than traditional resonant approaches, thus enabling much larger data throughput.**

***Index Terms*—Piezoelectric Micro-Machined Ultrasonic Transducers, pMUTs, Micro Electro-Mechanical Systems, MEMS, Resonators, Ultrasonic, Ultrasound, Communication, Underwater, Intrabody, Data-Links**

## I. Introduction

Piezoelectric Micro-Machined Ultrasonic Transducers (pMUTs) have been widely explored for medical imaging [1] [2], power transfer [3] [4], fingerprint sensors [5], microphones [6] [7], pressure sensors [8], etc. For underwater and intrabody communication, these devices have been less explored since their quality factor $Q$ [9] is lower compared to conventional Lead Zirconate Titanate transducers (PZTs) [10]. This directly translates into less transferred energy and less efficient communication. In this work, novel pMUT-based Acoustic Duplexers (PADs) that enable large data-rates and full-duplex operation for underwater and intrabody data-links are proposed.

The proposed PADs consist of two distributed matching filters, one for each individual transmission/receiving band. The distributed matching filters have the function to maximize the voltage gain on the pMUTs. The higher the voltage on the pMUTs, the higher the out-coupled acoustic pressure that those can generate will be. High acoustic pressure is needed to obtain strong signal at the receiver and therefore to maximize the Signal-to-Noise Ratio ($SNR$). Furthermore, given a desired $SNR$, longer transmission distances can be achieved by increasing the acoustic pressure of the radiating element.

This work was supported by NSF programs MRI-SEANet (NSF Number 1726512) and NeTS-Small (NSF Number 1618731).

In this work, two identical PAD prototypes are designed with lumped elements and fabricated on standard FR4 (glass epoxy) Printed Circuit Boards (PCBs). Each PAD is connected to a pMUTs array as radiating element, both for transmitting and receiving simultaneously. Each PAD is individually tested for its functionality and compared to the simulations.

The transmission capability of the PADs is tested underwater in a De-Ionized (DI) water tank as shown in Fig. 4. The two ports for the duplexers are connected to a Vector Network Analyzer (VNA) and transmission S-parameters are measured. Based on the results shown in Fig. 5, the transmission and receiving bandwidths can be characterized.

At this point, in order to demonstrate the full duplexing capability of the PADs, a communication protocol is added to the transmission setup. Instead of powering the duplexers with the VNA, a Universal Software Radio Peripheral (USRP) is used to implement a Orthogonal Frequency-Division Multiplexing (OFDM) with Binary Phase-Shift Keying (BPSK) and communicate between the two PADs. This configuration allows to measure the Bit-Error-Rate ($BER$) agains certain levels of $SNR$, that is determined by the signal strength sent by the USRP (Fig. 6).

Throughout the paper, the duplexer model, the transmission test, communication test and their results are presented. In conclusion, this work demonstrated, for the first time, a full-duplexing communication link for intrabody and underwater application, by using a pMUTs array as radiating element.

## II. pMUT Acoustic Duplexer (PAD) Model

The model of each duplexer consists of two band-pass Chebyshev filters. Each filter is designed with a different center frequency, $f_1 = 3.7MHz$ and $f_2 = 5.3MHz$, and bandwidths of $1MHz$. This filters differ from a standard LC-tree configuration because one of the series capacitance is replaced by the capacitance of the pMUTs array. The schematics are shown in Fig. 1a and the lumped element values are shown in the table in Fig. 1b. Furthermore, the filters are designed to maximize the voltage gain on the transducer and achieve a higher out-coupled acoustic pressure. Thus, better transmission capabilities are achieved than by directly feeding the signal from a $50\Omega$ terminal. The Printed Circuit Board (PCB) prototype of the duplexer is shown in Fig. 1c.

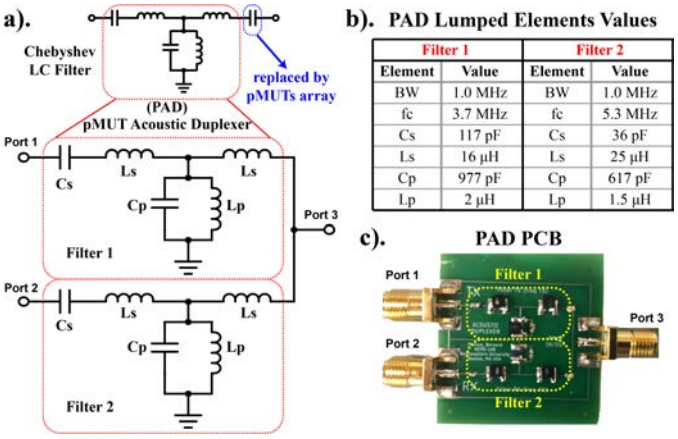


| Filter 1 | | Filter 2 | |
|---|---|---|---|
| Element | Value | Element | Value |
| BW | 1.0 MHz | BW | 1.0 MHz |
| fc | 3.7 MHz | fc | 5.3 MHz |
| Cs | 117 pF | Cs | 36 pF |
| Ls | 16 µH | Ls | 25 µH |
| Cp | 977 pF | Cp | 617 pF |
| Lp | 2 µH | Lp | 1.5 µH |

Fig. 1. a). At the top is shown a typical LC-tree configuration for a band-pass Chebyshev filter where the last series capacitance is replaced by the pMUT array capacitance. At the bottom is shown the configuration of the pMUT Acoustic Duplexer (PAD) used in this work. b). Table of the PAD lumped elements values for both modified band-pass Chebyshev filters. The filters are designed with center frequencies ($f_c$) $f_1 = 3.7MHz$ and $f_2 = 5.3MHz$ respectively, and bandwidths of $1MHz$ each. c). PCB of the PAD prototype used in this work. The two filters are highlighted with the yellow dashed line and the input (Port 1 and Port 2) and output (Port 3) ports are marked.

In order to correctly design the duplexers, circuit simulations are run. Those simulations also include the quality factor $Q$ of the lumped inductors, which is in the range of 30-50, which will limit the insertion loss (IL). An S-parameter analysis is run and the results are shown in Fig. 5, solid curves. The $S_{13}$ curve represents the transmission between Port 1 and Port 3 (filter at $f_1 = 3.7MHz$) and the $S_{23}$ curve represents the transmission between Port 2 and Port 3 (filter at $f_2 = 5.3MHz$). The average IL is $-7dB$, which is limited mainly by the low $Q$ of the inductors. This can be improved by replacing the lumped elements of the filters with micro-machined filters such as Cross-Sectional Lamé Mode Resonators (CLMRs) adapted to low frequency [11] [12], which exhibit $Qs > 1000$. Finally, the S-parameters are measured directly on the duplexer prototype with a good matching of the simulations (Fig. 5, dashed curves). The small mismatches are due to the discrepancy between the nominal values, used in the simulations, and the real values of the components, used in the circuits, and the PCB parasitic.

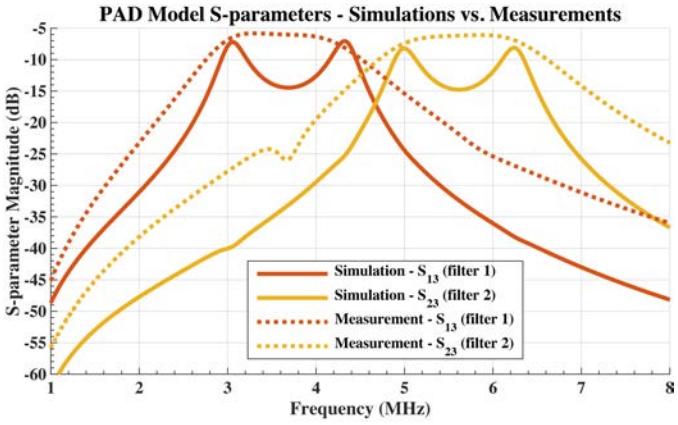


Fig. 2. S-parameter simulation (solid curves) and measurements (dashed curves) of the PAD. $S_{13}$ and $S_{23}$ are the transmission parameter of filter $f_1$ and $f_2$ respectively.

## III. pMUTs Array Fabrication

The fabrication of the pMUTs array follows the standard micro-machining steps of an Aluminum Nitride ($AlN$) device, as shown in Fig. 3a. The process starts with a $300\mu m$ silicon ($Si$) wafer on which $500nm$ of thermal oxide ($SiO_2$) are grown (i). Following, the bottom electrode is fabricated through the lift-off process. After patterning the photo-resist (PR), $150nm$ of platinum ($Pt$) are sputtered on the wafer and the wafer is sonicated in order to remove the unwanted metal. (ii). At this point, $750nm$ of $AlN$ are deposited and the piezoelectric layer is patterned for VIAs, which are etched with hot phosphoric acid, in order to allow access to the bottom electrode (iii). Moreover, the top electrode is also fabricated through the lift-off process. After patterning the PR, $150nm$ of gold ($Au$) are sputtered and the wafer is sonicated in order to remove the unwanted metal (iv). Finally, the pMUTs cavities are back-side etched through the Deep Reactive Ion-Etching (DRIE) process (v). An optical image of fabricated pMUTs array is shown in Fig. 3b and a Scanning Electron Microscope (SEM) image of a single pMUT is shown in Fig. 3c.

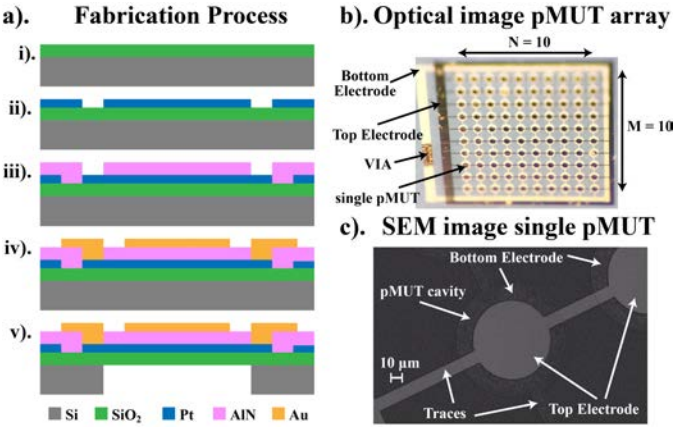


Fig. 3. a). pMUTs array fabrication process steps. (i) $SiO_2$ thermal growth. (ii) Bottom electrode deposition ($Pt$) and patterning. (iii) $AlN$ deposition. (iv) Top electrode deposition ($Au$) and patterning. (v) Backside etching to define the pMUTs cavity and membrane area. b). Optical image of a fabricated pMUTs array. The array is made by $N = 10$ columns and $M = 10$ arows, thus a 100 pMUTs in total. Top and bottom traces together with the the VIAs can be distinguished in the figure. c). Scanning Electron Microscope (SEM) image of a single pMUT. Top and bottom electrodes and traces together with the pMUT cavity can be distinguished in the figure.

## IV. Measurements Setup and Results

The measurements setup consists of a De-Ionized (DI) water tank in which the pMUTs arrays are immersed. Experiments can be performed directly on the pMUTs arrays and then compared to the results obtained by adding the duplexers to the system. Once the PADs are added to the system, two types of measurements can be performed. First of all, the PADs are connected to a Vector Network Analyzer (VNA) and a power transmission measurement is run. Furthermore, the PADs are connected each to a Universal Software Radio Peripherals (USRPs) and communication tests are run.

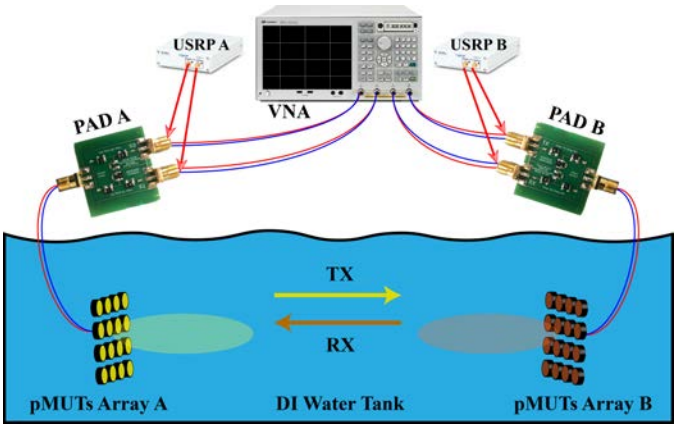


Fig. 4. Measurements setup. The pMUTs array are immersed in a DI water tank. PADs are connected to the pMUTs arrays and then connected to the relative instruments. Based on the measurements that need to be performed, the PADs are then connected to a VNA or to a USRP.

### A. Transmission Results

The power transmission of the full system has been characterized as shown in Fig. 5. First of all, the power transfer between two pMUTs arrays only is measured (blue dashed curve). This curve shows a flat broadband response since the quality factor of the array is very low in water ($Q < 50$). This allows margin for improvement with the PADs filters. In fact, once the duplexers are added to the pMUTs arrays, both the power transmission and frequency selectivity improves by rejecting the out-of-band signal (red and yellow curves).

The red curve is the transmission measurement between filter at center frequency $f_1$ of PAD A and filter at the same center frequency of PAD B. Similarly, the yellow curve is the transmission measurement between filter at center frequency $f_2$ of PAD A and filter at the same center frequency of PAD B. The out-of-band rejection can be further improved by cascading more of each filter in the duplexer or by changing the lumped components with CLMRs filters adapted to low frequency [11] [12].

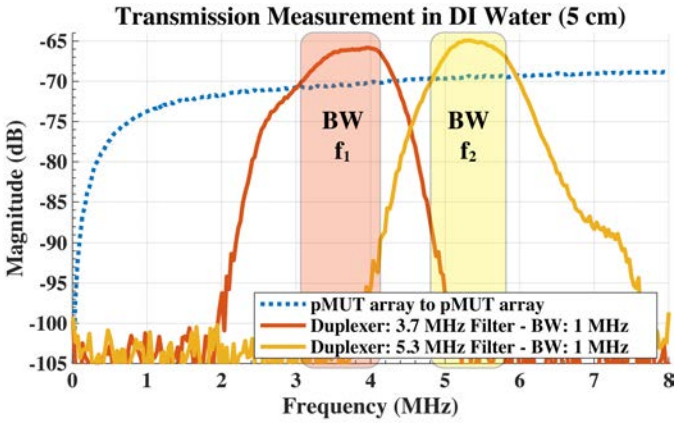


Fig. 5. Transmission measurements results. The blue dashed curve represents the transmission between the pMUTs array without the use of the duplexers (flat band). The solid red and solid yellow curves represent the transmission when the PADs are added to the system, respectively between the filters at center frequency $f_1$ and $f_2$. Here the power transmission improves and the bandwidths are well defined, thus frequency selectivity improves by rejecting the out-of-band signal.

### B. Communication Results

In order to test the communication capabilities of the novel pMUT acoustic duplexer, an Orthogonal Frequency-Division Multiplexing (OFDM) with Binary Phase-Shift Keying (BPSK) is implemented using two Universal Software Radio Peripherals (USRP). This demonstrates the capability of the duplexer to simultaneously transmit and receive on different bands using a single pMUTs array per duplexer as radiating element (Fig. 4). The results of the Bit-Error-Rate ($BER$) vs. the Signal-to-Noise Ratio ($SNR$) are shown in Fig. 6.

It is to notice that when the duplexers are added to the system, the $BER$ is improved, thus allowing better communication efficiency than when using directly the band of the pMUTs array. For the pMUT-to-pMUT only communication, it is possible to transmit and receive only in different time slots (half-duplex). Instead, when adding the PADs to the system, a full-duplexing communication capability is reached, allowing much higher data-rates. Furthermore, for levels of $BER < 10^{-4}$, standard videos can be transmitted [13] [14] [15].

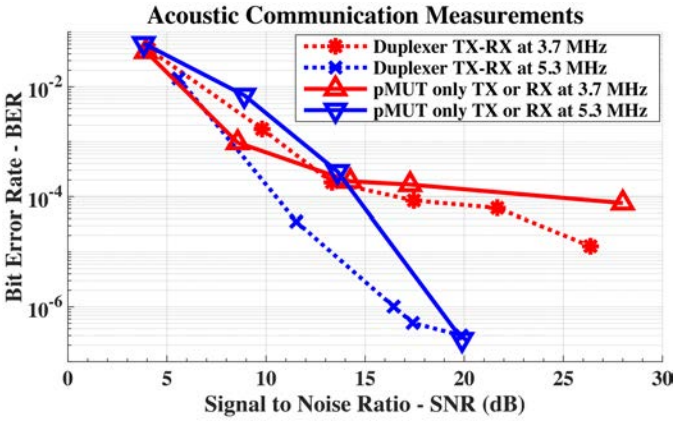


Fig. 6. Acoustic communication measurements of the Bit-Error-Rate ($BER$) vs. the Signal-to-Noise Ratio ($SNR$). The solid lines are the measurements with pMUTs arrays only while the dashed lines are the measurements with the duplexers added to the communication system. Red and blue lines are the communication results through the $f_1 = 3.7MHz$ and $f_2 = 5.3MHz$ bandwidths of the duplexer respectively. (TX = Transmit, RX = Receive)

## V. Conclusions

In conclusion, this works demonstrates, for the first time, an acoustic duplexer based on pMUTs array as radiating element. A first prototype has been realized and successfully characterized. The electrical circuit of the duplexer defines two different bandwidths, one to transmit and one to receive, directly on a single pMUTs array, which allows a full-duplexing capability. With this approach, a high out-of-band rejection and voltage amplification is achieved on the transducer. The duplexers have been characterized and a full-duplexing communication scheme has been implemented do demonstrate this approach. Once the OFDM scheme with a BPSK encoding is used, the $BER$ vs. $SNR$ can be measured to determine the quality of the communication. In the end, very good $BER$ values ($< 10^{-4}$) are achieved that will allow full-duplex video streaming directly through the pMUTs.

## REFERENCES


[1] C. Sun, F. Dai, S. Jiang, and Y. Liu, "A novel single-element dual-frequency ultrasound transducer for image-guided precision medicine," in *Ultrasonics Symposium (IUS), 2017 IEEE International*, pp. 1–4, IEEE, 2017.

[2] K. Smyth, C. Sodini, and S.-G. Kim, "High electromechanical coupling piezoelectric micro-machined ultrasonic transducer (pmut) elements for medical imaging," in *Solid-State Sensors, Actuators and Microsystems (TRANSDUCERS), 2017 19th International Conference on*, pp. 966–969, IEEE, 2017.

[3] E. Mehdizadeh and G. Piazza, "Aln on soi pmuts for ultrasonic power transfer," in *Ultrasonics Symposium (IUS), 2017 IEEE International*, pp. 1–4, IEEE, 2017.

[4] T. C. Chang, M. J. Weber, J. Charthad, S. Baltsavias, and A. Arbabian, "End-to-end design of efficient ultrasonic power links for scaling towards sub-millimeter implantable receivers," *IEEE transactions on biomedical circuits and systems*, 2018.

[5] X. Jiang, H.-Y. Tang, Y. Lu, E. J. Ng, J. M. Tsai, B. E. Boser, and D. A. Horsley, "Ultrasonic fingerprint sensor with transmit beamforming based on a pmut array bonded to cmos circuitry," *IEEE transactions on ultrasonics, ferroelectrics, and frequency control*, vol. 64, no. 9, pp. 1401–1408, 2017.

[6] Y. Kusano, J. Segovia-Fernandez, S. Sonmezoglu, R. Amirtharajah, and D. A. Horsley, "Frequency selective mems microphone based on a bioinspired spiral-shaped acoustic resonator," in *Solid-State Sensors, Actuators and Microsystems (TRANSDUCERS), 2017 19th International Conference on*, pp. 71–74, IEEE, 2017.

[7] J. Segovia-Fernandez, S. Sonmezoglu, S. Block, Y. Kusano, J. Tsai, R. Amirtharajah, and D. Horsley, "Monolithic piezoelectric aluminum nitride mems-cmos microphone," in *Solid-State Sensors, Actuators and Microsystems (TRANSDUCERS), 2017 19th International Conference on*, pp. 414–417, IEEE, 2017.

[8] M. J. Weber, Y. Yoshihara, A. Sawaby, J. Charthad, T. C. Chang, and A. Arbabian, "A miniaturized single-transducer implantable pressure sensor with time-multiplexed ultrasonic data and power links," *IEEE Journal of Solid-State Circuits*, vol. 53, no. 4, pp. 1089–1101, 2018.

[9] Q. Wang and D. A. Horsley, "Using a mutual acoustic impedance model to improve the time domain response of pmut arrays," in *Ultrasonics Symposium (IUS), 2017 IEEE International*, pp. 1–4, IEEE, 2017.

[10] J. Jung, V. Annapureddy, G.-T. Hwang, Y. Song, W. Lee, W. Kang, J. Ryu, and H. Choi, "31-mode piezoelectric micromachined ultrasonic transducer with pzt thick film by granule spraying in vacuum process," *Applied Physics Letters*, vol. 110, no. 21, p. 212903, 2017.

[11] C. Cassella, Y. Hui, Z. Qian, G. Hummel, and M. Rinaldi, "Aluminum nitride cross-sectional lamé mode resonators," *Journal of Microelectromechanical Systems*, vol. 25, no. 2, pp. 275–285, 2016.

[12] C. Cassella, G. Chen, Z. Qian, G. Hummel, and M. Rinaldi, "Cross-sectional lamé mode ladder filters for uhf wideband applications," *IEEE Electron Device Letters*, vol. 37, no. 5, pp. 681–683, 2016.

[13] E. Demirors, G. Sklivanitis, T. Melodia, S. N. Batalama, and D. A. Pados, "Software-defined underwater acoustic networks: toward a high-rate real-time reconfigurable modem," *IEEE Communications Magazine*, vol. 53, no. 11, pp. 64–71, 2015.

[14] E. Demirors, G. Sklivanitis, G. E. Santagati, T. Melodia, and S. N. Batalama, "Design of a software-defined underwater acoustic modem with real-time physical layer adaptation capabilities," in *Proceedings of the International Conference on Underwater Networks & Systems*, p. 25, ACM, 2014.

[15] E. Demirors, J. Shi, A. Duong, N. Dave, R. Guida, B. Herrera, F. Pop, G. Chen, C. Cassella, S. Tadayon, *et al.*, "The seanet project: Toward a programmable internet of underwater things," in *IEEE Underwater Communications Conf. and Workshop (UComms)*, 2018.